Do we swallow the waste from our brain?

Joshua Leaston
Imaginostics Inc
Praveen Kulkarni
Northeastern University
Codi Gharagouzloo
Imaginostics Inc
Ju Qiao
Northeastern University
Nicole Bens
Northeastern University
Craig Ferris (c.ferris@northeastern.edu)
Northeastern University https://orcid.org/0000-0001-9744-5214

Article

Keywords: ferumoxytol, magnetic resonance imaging, waste

Posted Date: July 9th, 2021

DOI: https://doi.org/10.21203/rs.3.rs-679275/v1

Version of Record: A version of this preprint was published at Frontiers in Neuroscience on November 23rd, 2021. See the published version at https://doi.org/10.3389/fnins.2021.763780.

Do we swallow the waste from our brain?

Joshua Leaston[1*], Praveen Kulkarni [2*], Codi Gharagouzloo[1,2], Ju Qiao[2], Nicole Bens[2], , Craig F. Ferris[2,3]

[1] Imaginostics, Inc., Cambridge, Massachusetts; [2] Center for Translational Neuroimaging, Northeastern University, Boston, Massachusetts; [3]Departments of Psychology and Pharmaceutical Sciences, Northeastern University, Boston, Massachusetts

* Both share equal authorship

Address all Correspondence to:

Craig Ferris, PhD, Director Center for Translational NeuroImaging; 360 Huntington Ave, Boston Massachusetts, 02115; Email: c.ferris@northeastern.edu; Phone:508 259 4908

Conflict of Interest

C.F.F has a financial interest in Animal Imaging Research, the company that makes the radiofrequency electronics and holders for awake animal imaging. C.A.G. has financial interest in Imaginostics, a company commercializing neuroimaging biomarkers of the vascular and perivascular spaces.

Abstract

Ferumoxytol an iron oxide nanoparticle was infused into the lateral cerebroventricle of awake rats to follow its movement and clearance from the brain using magnetic resonance imaging. Within minutes the contrast agent could be observed accumulating on the soft palate at the back of the throat. In a subsequent study fluorescent quantum dots were infused into the brain of rats and within 15 min could be observed in the esophagus using microscopy. These imaging studies clearly show the gut is helping to clear waste from the brain.

In a recent study we infused a small molecular weight magnetic resonance imaging (MRI) contrast agent (CA) gadobenate dimeglumine (1.06-kDa) into the lateral cerebral ventricle (LCV) of awake rats during the scanning session and mapped the site-specific movement of trace from the perivascular system into the surrounding brain parenchyma (1). This study provided clear evidence of circadian regulation of perivascular clearance that was greatest during the light-phase (rat normal rest/sleep phase) but independent of sleep (2). The present study was designed to repeat this study but with a much larger MRI CA ferumoxytol (731-kD) with the intention of mapping the site-specific changes in the perivascular volume over the circadian light-dark cycle. Ferumoxytol is used with quantitative ultra-short time-to-echo, contrast-enhanced (QUTE-CE) MRI, a technology we developed to measure microvascular density and function in awake rats using optimized 3D UTE MRI and intravascular CA (3, 4). We assumed the ferumoxytol, a superparamagnetic iron oxide nanoparticle (SPION) with a dextran coating, and 23 nm hydrodynamic diameter would be confined to the cerebrospinal fluid (CSF) and provide contrast as it traversed the cerebroventricular system, meninges, and perivascular spaces of the brain (5, 6). Indeed, ferumoxytol is an excellent blood pool CA because it does not cross the blood brain barrier. To our surprise, the ferumoxytol appeared outside the brain within minutes after administration accumulating on the soft palate at the back of the throat.

This observation was made in six rats with cannula placements in the LCV and infused with 10 µl of ferumoxytol (6 µg/µl Fe) during the MRI scanning session while fully awake. QUTE-CE images were collected continuously at 7 min blocks for a duration of 70 min. All imaging was done during the light-phase of the light-dark cycle. Shown in **Fig 1** are sagittal sections from one rat depicting the accumulation and localization of ferumoxytol signal following intracerebroventricular (ICV) infusion. All rats tested showed a similar signal profile (see **Supplementary Data Fig S1**). The images in **Fig 1a**. are a times series of voxel based Maximum Intensity Projections (MIPs) made from the sagittal view of the entire rat head taken at 7 min intervals. The color scale represents the contrast-noise-ratio, as defined by the signal-noise-ratio post-contrast, subtracted by the signal-noise-ratio pre-contrast. Note the accumulation of ferumoxytol at the soft palate, olfactory bulb, and subarachnoid space (SAS) over time. Interestingly, trace can be observed accumulating on the soft palate as early as 7 min post ICV infusion attesting to its rapid clearance from the brain. The appearance of trace

outside the brain in blood or lymph nodes following injection ICV, intrathecally, or into different brain regions, has been reported in numerous studies. However, most CSF clearance studies in animals have been performed under anesthesia with reports of trace appearing in blood and lymph nodes between 30-180 min post administration, e.g. dog (7), rabbit (8-11), cat (11, 12), mouse (13-16), rat (17-21).

Fig 1b. shows a summary image of all the scans from all six rats using a voxel threshold contrast-to-noise ratio greater than five. These data are mapped onto the corresponding average anatomical image for all rats. Note the injection site in the LCV. Ferumoxytol accumulates along the base of the brain in the subarachnoid space while there is no evidence of accumulation of CA on the dorsal surface of the brain as noted in previous studies (13). The presence of CA on the rostral surface of the olfactory bulb reflects the movement from the subarachnoid space through the cribriform plates and below into the nasal epithelium and possibly the nasal cavity. The olfactory route of CSF clearance through the cribriform plate and into nasal mucosal lymphatics to deep cervical lymph nodes is well documented across multiple mammalian species (8-12, 14, 17, 21-25) Contrast agent can be seen all along the boundaries of the nasal pharynx leading down to the soft palate and oral/nasal passage. **Fig 1c.,** rendered in 3D-Slicer (26) shows an average QUTE-CE image generated from 10 scans with a transparent overlay of the brain for anatomical reference (70 minutes of image acquisition time). This 3D summary of ferumoxytol movement and localization following ICV infusion highlights the cerebroventricular system, the caudal/rostral extent of the subarachnoid space, movement across the olfactory bulb and into the nasal cavity, down the nasal pharynx to soft palate and oral/nasal passage.

The localization of ferumoxytol to anatomical brain areas is better shown in **Fig 2**. where the accumulation of CA is mapped onto high resolution MRI images. The most rostral section **2a**. shows CA around the nasal turbinates and nasal pharynx. Caudal sections **2b**. through **2e**. show CA along the basal lateral subarachnoid space and cisterns. There is CA around the nasal pharynx (**2b, c**.) with accumulation starting on the soft palate (**2c**.) and oral pharynx (**2d.**). The most caudal section **2e**. shows CA around the subarachnoid space at the level of the cerebellum and medulla but missing from trachea and esophagus. The field of view during the scanning session did not allow for imaging of the deep cervical lymph nodes which would have been further caudal to section **2e**. This visual record of ferumoxytol accumulation over

the first hr after ICV infusion was similar across all six rats tested (**Supplementary Data Fig S2**).

Clearance through the Nasal Cavity

All studies to date have assumed that CSF leaving through the cribriform plates is taken up by the lymphatic vessels in the mucosal lining of the nasal turbinates to eventually finds its way back to the systemic venous circulation (27). Could contents from the CSF appear in nasal exudate? Healthy dogs show leakage of CSF into the nasal cavity that can be followed by imaging of CA injected into the brain (28). This phenomenon is thought to be an anomaly unique to dogs and give the name rhinorrhea. However, recent studies in humans have shown swabs of nasal exudates can be used to assess the differences in iron levels following brain damage from ischemic or hemorrhagic strokes (29) and amyloid beta from nasal secretions of patients with Alzheimer's dementia (30). It is not surprising that biomarkers from the brain can appear in the mucus of the nasal cavity given the success of drug delivery to the brain across the same mucus boundary (31). Drugs given intranasally gain rapid access to the brain, and what is not absorbed is simply swallowed (31). Indeed, any brain derived, or exogenously inhaled material found in the mucus of the nasal cavity would be expected to move down the nasal pharynx helped by the propulsion of microcilia to eventually meet with the oral pharynx at the back of the throat. This raises an intriguing question. Could these rats in our study be swallowing a portion of ferumoxytol cleared from their brain? Previous studies have searched systemic and lymphatic circulations to account for trace injected into the brain and can only account for less than half of what is administered (12). Perhaps the missing trace ends up in the gastrointestinal tract.

Finding Brain Derived Trace in the Esophagus

If the CA was being swallowed by awake rats during the scanning session, it should appear in the esophagus. To test this hypothesis we ran a series of studies on female and male rats using quantum dots (Qdot® 605 ITK™ amino (PEG) with a hydrodynamic diameter of 16-20 nm. While under light isoflurane anesthesia three female rats were infused for two min with 20 µl of Qdots into the LCV. One female and one male rat were infused with 10 µl of Qdots mirroring the QUTE-CE imaging protocol. One male rat was infused with 0.9% NaCl vehicle at 10 µl/min and one male was given a 1 µl injection of Qdots into each nostril. They were allowed to awaken and between 15- and 40-min post infusion, euthanized, and the upper

esophagus removed, bisected along the long axis on a microscope slide, and the tissue compressed under a coverslip. Slides were imaged using a Zeiss LSM 880 confocal microscope equipped with a Plan-Apochromat 63x/1.4 Oil DIC M27 objective. The Quantum Dots were excited with a 405 laser at 10% laser power. Accompanying the fluorescent image was a T-PMT image acquired to provide context and locational information within the tissue sample.

Figure 3 shows a collage of the fluorescent images with two representative examples of each experiment at different time points. The red signal associated with the long linear threads and twisted strands (white arrows) is presumably Qdots adhering to polymers of mucin glycoproteins. Mucus glycoproteins behave as a polyanionic polyelectrolyte that can readily hydrate and bind to cationic ions (32, 33). Qdot® 605 ITK™ amino with its net positive charge could be acting as a counter ion helping to bind to the mucin. Note the presence of Qdots as early as 15 min post ICV infusion (**Fig 3a**.) The upper esophagus collected from a male rat infused ICV with 10 µl of saline (**Fig 3b**.) showed no evidence of red fluorescent signal while the esophagus of a male injected with 1 µl of Qdot into each nostril (**Fig 3c.**) is replete with red fluorescent signal organized in threads and strands that matches the images from ICV infused Qdot.

Something so Obvious

Why is the evidence so clear that ICV injected CA accumulates on the soft palate and oral/nasal pharynx with MRI, yet has never been reported before? While there are probably multiple reasons we will focus on three.

Attention Elsewhere: Anything escaping from the systemic circulation is taken up by the lymphatic vessels, acted upon by the reticuloendothelial system of lymph nodes and recycled to the venous circulation. The original reports of CNS tracers appearing in the cervical lymph nodes across different species mirrored what was happening in the periphery and fulfilled an expectation (34). One would not be expected to look in the gut for CSF waste when all the attention was justifiably focused on the cervical lymph nodes. To this point, Xray imaging of CSF outflow 30 min after cisternal infusion of CA in rabbits shows signal in lymph nodes in addition to the soft palate, but the latter was not discussed (9). ICV injection of Combidex, a dextran-coated SPION MRI CA in rats shows signal in lymph nodes and an ostensible amount

of signal around the soft palate and oral pharynx. Images from this study are shown in **Supplementary Data Fig S3** depicting the injection site of CA into brain parenchyma and ICV. Both routes of administration present with bright signal below the trachea localized to the soft palate and oral pharynx. Yet again, this signal contrast was not addressed in the study.

Confound of Anesthesia: Nearly all studies cited in this article, and others from reviews of perivascular clearance, report the use of anesthesia. ICV infused MRI CA comes to equilibrium across the brain within 30-40 min in the awake rat (1) and is rapidly cleared from the mouse brain within 15-30 min (22) but under anesthesia these processes may take hrs (35-38) . How much of the clearance of CA is delayed or redirected using anesthesia (2, 39)? Here we show Qdots are rapidly moved to the nasal cavity, presumably collected in mucus, and propelled by mucocilliary action down the nasal pharynx to the back of the throat where they appear in the esophagus – as early as 15 min post ICV infusion. Concentrating the rapidly cleared ferumoxytol along the nasal pharynx and soft palate improves its visibility.

QUTE-CE Imaging: QUTE-CE MRI is a recently patented imaging technology developed for quantitative vascular imaging optimized with 3D Ultra-Short Time-to-Echo (UTE) pulse sequences with intravascular ferumoxytol to produce positive contrast angiographic images unparalleled to time-of-flight imaging or gadolinium-based first-pass imaging (3, 40). We recently published a study mapping the absolute physiological cerebral blood volume (CBV) of the awake rat brain, including measurements of microvascular density, vascular functional reserve and CBV modulation with anesthesia (4). This more sensitive MRI technology combined with ICV infusion and rapid accumulation of ferumoxytol in the back of the throat under awake conditions would be the most probable explanation for the observations made in this study.

Summary

As noted above, efforts to recover tracer injected into the brain could only account for 50% or less using measurements taken from blood and lymphatics (12). Our finding that rats swallow trace infused into their brain CSF could explain the missing 50%. However, and more importantly, do humans swallow the waste from their brain CSF? The examples provided above using nasal swabs to presumably sample biomarkers coming from the brain are suggestive but not convincing (29, 30). Perivascular clearance in humans is greatest during

the dark-phase of the circadian light-dark cycle during rest and sleep. Mucus accumulates along the nasopharynx during sleep. The morning accumulation of mucus at the back of the throat may offer a rich source of brain biomarkers.

Acknowledgments

We thank Drs.Gouxin Rong, Alex Lovely and Heather Clark for their expertise in fluorescent microscopy and the microscopy resources at the Chemical Imaging of Living Systems Institute.

Declarations

Ethics approval and consent to participate
Not applicable.

Consent for publication
Yes

Competing interests.

C.F.F has a financial interest in Animal Imaging Research, the company that makes the radiofrequency electronics and holders for awake animal imaging. C.A.G. has financial interest in Imaginostics, a company commercializing neuroimaging biomarkers of the vascular and perivascular spaces.

Funding

No funding

Authors' contributions
All of the authors have contributed substantially to the manuscript. All authors have read and agreed to the published version of the manuscript.

Concept, drafting and interpretation – Ferris, Kulkarni, Gharagouzloo, Leaston

Execution and analysis – Leaston, Kulkarni, Qiao, Gharagouzloo, Bens

Bibliography

1. Cai X, Qiao J, Kulkarni P, Harding IC, Ebong E, Ferris CF (2020): Imaging the effect of the circadian light-dark cycle on the glymphatic system in awake rats. *Proc Natl Acad Sci U S A*. 117:668-676 10.1073/pnas.1914017117.
2. Ferris CF (2021): Rethinking the Conditions and Mechanism for Glymphatic Clearance. *Frontiers in neuroscience*. 15:624690 10.3389/fnins.2021.624690.PMC8060639.
3. Gharagouzloo CA, McMahon PN, Sridhar S (2015): Quantitative contrast-enhanced MRI with superparamagnetic nanoparticles using ultrashort time-to-echo pulse sequences. *Magn Reson Med*. 74:431-441 10.1002/mrm.25426.
4. Gharagouzloo CA, Timms L, Qiao J, Fang Z, Nneji J, Pandya A, et al. (2017): Quantitative vascular neuroimaging of the rat brain using superparamagnetic nanoparticles: New insights on vascular organization and brain function. *NeuroImage*. 163:24-33 10.1016/j.neuroimage.2017.09.003.PMC5824692.
5. Pizzo ME, Wolak DJ, Kumar NN, Brunette E, Brunnquell CL, Hannocks MJ, et al. (2018): Intrathecal antibody distribution in the rat brain: surface diffusion, perivascular transport and osmotic enhancement of delivery. *J Physiol*. 596:445-475 10.1113/JP275105.PMC5792566.
6. Abbott NJ, Pizzo ME, Preston JE, Janigro D, Thorne RG (2018): The role of brain barriers in fluid movement in the CNS: is there a 'glymphatic' system? *Acta neuropathologica*. 135:387-407 10.1007/s00401-018-1812-4.
7. Di Chiro G, Girton ME, Frank JA, Dietz MJ, Gansow OA, Wright DC, et al. (1986): Cerebrospinal fluid rhinorrhea: depiction with MR cisternography in dogs. *Radiology*. 160:221-222 10.1148/radiology.160.1.3715036.
8. Bradbury MW, Cserr HF, Westrop RJ (1981): Drainage of cerebral interstitial fluid into deep cervical lymph of the rabbit. *The American journal of physiology*. 240:F329-336 10.1152/ajprenal.1981.240.4.F329.
9. Liu H, Ni Z, Chen Y, Wang D, Qi Y, Zhang Q, et al. (2012): Olfactory route for cerebrospinal fluid drainage into the cervical lymphatic system in a rabbit experimental model. *Neural regeneration research*. 7:766-771 10.3969/j.issn.1673-5374.2012.10.009.PMC4345659.

10. Yamada S, DePasquale M, Patlak CS, Cserr HF (1991): Albumin outflow into deep cervical lymph from different regions of rabbit brain. *The American journal of physiology*. 261:H1197-1204 10.1152/ajpheart.1991.261.4.H1197.
11. Pile-Spellman JM, McKusick KA, Strauss HW, Cooney J, Taveras JM (1984): Experimental in vivo imaging of the cranial perineural lymphatic pathway. *AJNR American journal of neuroradiology*. 5:539-545.
12. Bradbury MW, Cole DF (1980): The role of the lymphatic system in drainage of cerebrospinal fluid and aqueous humour. *J Physiol*. 299:353-365 10.1113/jphysiol.1980.sp013129.PMC1279229.
13. Ahn JH, Cho H, Kim JH, Kim SH, Ham JS, Park I, et al. (2019): Meningeal lymphatic vessels at the skull base drain cerebrospinal fluid. *Nature*. 572:62-66 10.1038/s41586-019-1419-5.
14. Aspelund A, Antila S, Proulx ST, Karlsen TV, Karaman S, Detmar M, et al. (2015): A dural lymphatic vascular system that drains brain interstitial fluid and macromolecules. *The Journal of experimental medicine*. 212:991-999 10.1084/jem.20142290.PMC4493418.
15. Ma Q, Ineichen BV, Detmar M, Proulx ST (2017): Outflow of cerebrospinal fluid is predominantly through lymphatic vessels and is reduced in aged mice. *Nat Commun*. 8:1434 10.1038/s41467-017-01484-6.PMC5681558.
16. Moinuddin SM, Tada T (2000): Study of cerebrospinal fluid flow dynamics in TGF-beta 1 induced chronic hydrocephalic mice. *Neurological research*. 22:215-222 10.1080/01616412.2000.11741064.
17. Walter BA, Valera VA, Takahashi S, Ushiki T (2006): The olfactory route for cerebrospinal fluid drainage into the peripheral lymphatic system. *Neuropathology and applied neurobiology*. 32:388-396 10.1111/j.1365-2990.2006.00737.x.
18. Saija A, Polidori C, Massi M, Perfumi M, De Caro G, Costa G (1989): Label distribution after injection of labelled tachykinins into the rat lateral cerebroventricle. *Res Commun Chem Pathol Pharmacol*. 64:99-110.
19. Vega JL, Jonakait GM (2004): The cervical lymph nodes drain antigens administered into the spinal subarachnoid space of the rat. *Neuropathology and applied neurobiology*. 30:416-418 10.1111/j.1365-2990.2004.00575.x.

20. Szentistvanyi I, Patlak CS, Ellis RA, Cserr HF (1984): Drainage of interstitial fluid from different regions of rat brain. *The American journal of physiology*. 246:F835-844 10.1152/ajprenal.1984.246.6.F835.
21. Kida S, Pantazis A, Weller RO (1993): CSF drains directly from the subarachnoid space into nasal lymphatics in the rat. Anatomy, histology and immunological significance. *Neuropathology and applied neurobiology*. 19:480-488 10.1111/j.1365-2990.1993.tb00476.x.
22. Ma Q, Ries M, Decker Y, Muller A, Riner C, Bucker A, et al. (2019): Rapid lymphatic efflux limits cerebrospinal fluid flow to the brain. *Acta neuropathologica*. 137:151-165 10.1007/s00401-018-1916-x.PMC6338719.
23. Johnston M, Zakharov A, Papaiconomou C, Salmasi G, Armstrong D (2004): Evidence of connections between cerebrospinal fluid and nasal lymphatic vessels in humans, non-human primates and other mammalian species. *Cerebrospinal Fluid Res*. 1:2 10.1186/1743-8454-1-2.PMC546409.
24. Boulton M, Young A, Hay J, Armstrong D, Flessner M, Schwartz M, et al. (1996): Drainage of CSF through lymphatic pathways and arachnoid villi in sheep: measurement of 125I-albumin clearance. *Neuropathology and applied neurobiology*. 22:325-333 10.1111/j.1365-2990.1996.tb01111.x.
25. Norwood JN, Zhang Q, Card D, Craine A, Ryan TM, Drew PJ (2019): Anatomical basis and physiological role of cerebrospinal fluid transport through the murine cribriform plate. *Elife*. 810.7554/eLife.44278.PMC6524970.
26. Fedorov A, Beichel R, Kalpathy-Cramer J, Finet J, Fillion-Robin JC, Pujol S, et al. (2012): 3D Slicer as an image computing platform for the Quantitative Imaging Network. *Magn Reson Imaging*. 30:1323-1341 10.1016/j.mri.2012.05.001.PMC3466397.
27. Proulx ST (2021): Cerebrospinal fluid outflow: a review of the historical and contemporary evidence for arachnoid villi, perineural routes, and dural lymphatics. *Cell Mol Life Sci*. 78:2429-2457 10.1007/s00018-020-03706-5.PMC8004496.
28. Di Chiro G, Stein SC, Harrington T (1972): Spontaneous cerebrospinal fluid rhinorrhea in normal dogs. Radioisotope studies of an alternate pathway of CSF drainage. *J Neuropathol Exp Neurol*. 31:447-453 10.1097/00005072-197207000-00004.
29. Garcia-Cabo C, Llano-Suarez P, Benavente-Fernandez L, Calleja-Puerta S, Costa-Fernandez JM, Fernandez-Abedul MT (2020): Obtaining information from the brain in a non-

invasive way: determination of iron in nasal exudate to differentiate hemorrhagic and ischemic strokes. *Clin Chem Lab Med*. 58:847-853 10.1515/cclm-2019-0899.

30. Kim YH, Lee SM, Cho S, Kang JH, Minn YK, Park H, et al. (2019): Amyloid beta in nasal secretions may be a potential biomarker of Alzheimer's disease. *Scientific reports*. 9:4966 10.1038/s41598-019-41429-1.PMC6428828.

31. Pardeshi CV, Belgamwar VS (2013): Direct nose to brain drug delivery via integrated nerve pathways bypassing the blood-brain barrier: an excellent platform for brain targeting. *Expert opinion on drug delivery*. 10:957-972 10.1517/17425247.2013.790887.

32. Thornton DJ, Rousseau K, McGuckin MA (2008): Structure and function of the polymeric mucins in airways mucus. *Annu Rev Physiol*. 70:459-486 10.1146/annurev.physiol.70.113006.100702.

33. Davies JR, Herrmann A, Russell W, Svitacheva N, Wickstrom C, Carlstedt I (2002): Respiratory tract mucins: structure and expression patterns. *Novartis Foundation symposium*. 248:76-88; discussion 88-93, 277-282.

34. Age-Dependent Impairment of Mitochondrial Function in Primate Brain - Bowling - 2006 - Journal of Neurochemistry - Wiley Online Library.

35. Li L, Chopp M, Ding G, Davoodi-Bojd E, Zhang L, Li Q, et al. (2020): MRI detection of impairment of glymphatic function in rat after mild traumatic brain injury. *Brain Res*. 1747:147062 10.1016/j.brainres.2020.147062.

36. Christensen J, Wright DK, Yamakawa GR, Shultz SR, Mychasiuk R (2020): Repetitive Mild Traumatic Brain Injury Alters Glymphatic Clearance Rates in Limbic Structures of Adolescent Female Rats. *Scientific reports*. 10:6254 10.1038/s41598-020-63022-7.PMC7148360.

37. Iliff JJ, Lee H, Yu M, Feng T, Logan J, Nedergaard M, et al. (2013): Brain-wide pathway for waste clearance captured by contrast-enhanced MRI. *The Journal of clinical investigation*. 123:1299-1309 10.1172/JCI67677.3582150.

38. Ding G, Chopp M, Li L, Zhang L, Davoodi-Bojd E, Li Q, et al. (2018): MRI investigation of glymphatic responses to Gd-DTPA infusion rates. *Journal of neuroscience research*. 96:1876-1886 10.1002/jnr.24325.PMC6186187.

39. Gakuba C, Gaberel T, Goursaud S, Bourges J, Di Palma C, Quenault A, et al. (2018): General Anesthesia Inhibits the Activity of the "Glymphatic System". *Theranostics*. 8:710-722 10.7150/thno.19154.PMC5771087.
40. Knobloch G, Colgan T, Schiebler ML, Johnson KM, Li G, Schubert T, et al. (2019): Comparison of gadolinium-enhanced and ferumoxytol-enhanced conventional and UTE-MRA for the depiction of the pulmonary vasculature. *Magn Reson Med*. 82:1660-1670 10.1002/mrm.27853.PMC6660410.
41. Kilkenny C, Browne W, Cuthill IC, Emerson M, Altman DG, Group NCRRGW (2010): Animal research: reporting in vivo experiments: the ARRIVE guidelines. *Br J Pharmacol*. 160:1577-1579 10.1111/j.1476-5381.2010.00872.x.PMC2936830.
42. Ferris CF, Smerkers B, Kulkarni P, Caffrey M, Afacan O, Toddes S, et al. (2011): Functional magnetic resonance imaging in awake animals. *Reviews in the neurosciences*. 22:665-674 10.1515/RNS.2011.050.
43. Febo M, Segarra AC, Tenney JR, Sullivan R, Brevard M, Duong TQ, et al. (2004): Imaging cocaine-induced changes in the reward system in conscous rate. *Journal of neuroscience methods*. 139:167-176.
44. Ferris CF, Yee JR, Kenkel WM, Dumais KM, Moore K, Veenema AH, et al. (2015): Distinct BOLD Activation Profiles Following Central and Peripheral Oxytocin Administration in Awake Rats. *Frontiers in behavioral neuroscience*. 9:245 10.3389/fnbeh.2015.00245.PMC4585275.
45. Yang L, Kress BT, Weber HJ, Thiyagarajan M, Wang B, Deane R, et al. (2013): Evaluating glymphatic pathway function utilizing clinically relevant intrathecal infusion of CSF tracer. *Journal of translational medicine*. 11:107 10.1186/1479-5876-11-107.3665671.
46. Muldoon LL, Varallyay P, Kraemer DF, Kiwic G, Pinkston K, Walker-Rosenfeld SL, et al. (2004): Trafficking of superparamagnetic iron oxide particles (Combidex) from brain to lymph nodes in the rat. *Neuropathology and applied neurobiology*. 30:70-79 10.1046/j.0305-1846.2003.00512.x.

Figure 1. Sagittal reconstructions of ferumoxytol movement and accumulation
The time series (a.) are images from a single rat collected at 7 min intervals over 70 min showing accumulation of CA along the soft palate over time. A summary image (b.) generated as an average of CA signal from six rats is mapped onto the T2 weighted anatomy image of the brain. The 3D reconstruction of CA within and outside the brain was generated from a single rat, postmortem, at the end of the imaging study to eliminate the artifact of blood vessels.

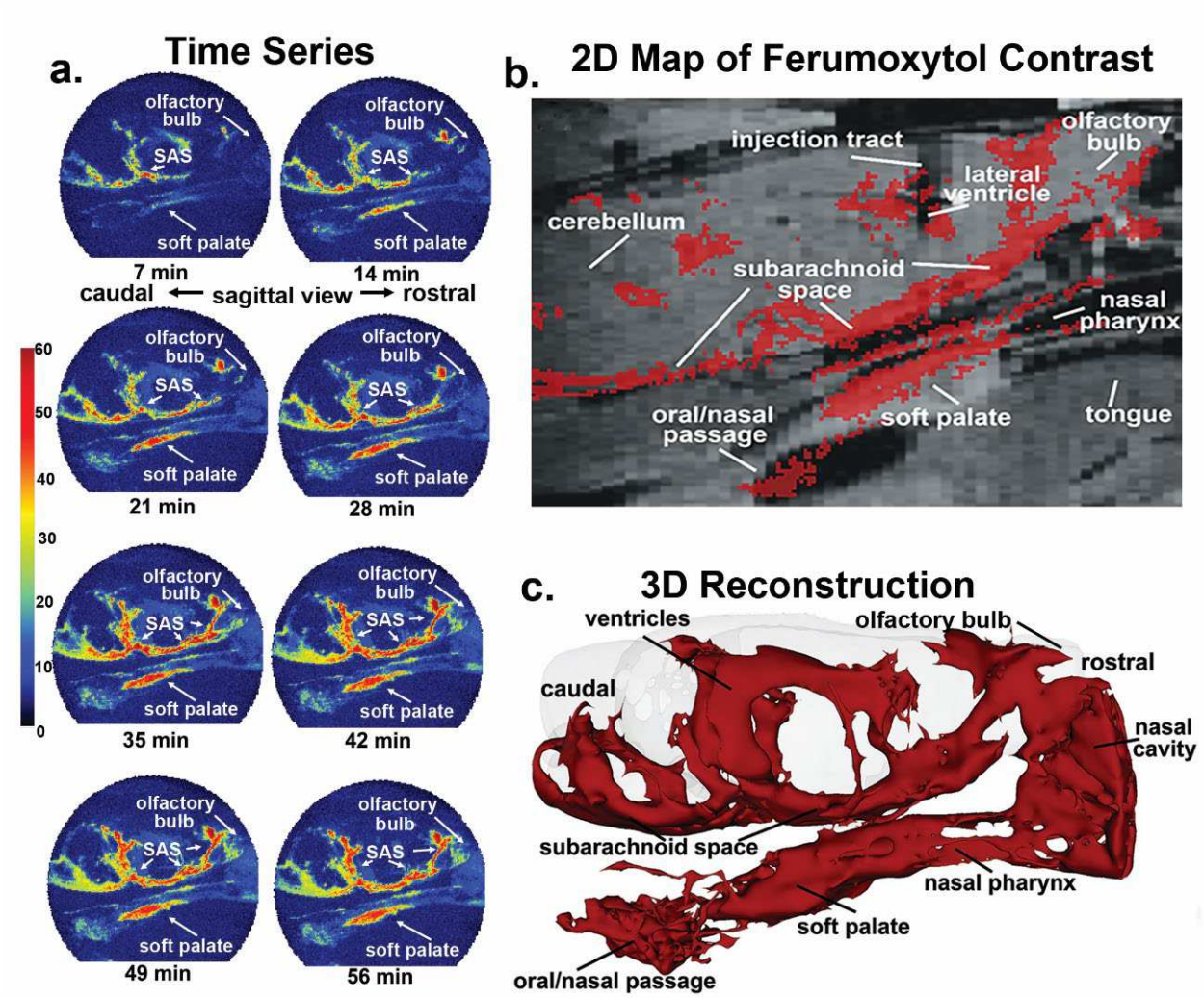

Figure 2. Mapping ferumoxytol signal

Shown are axial sections depicting the localization of the average CA signal from six rats mapped onto T2 weighted anatomy images of the rat brain.

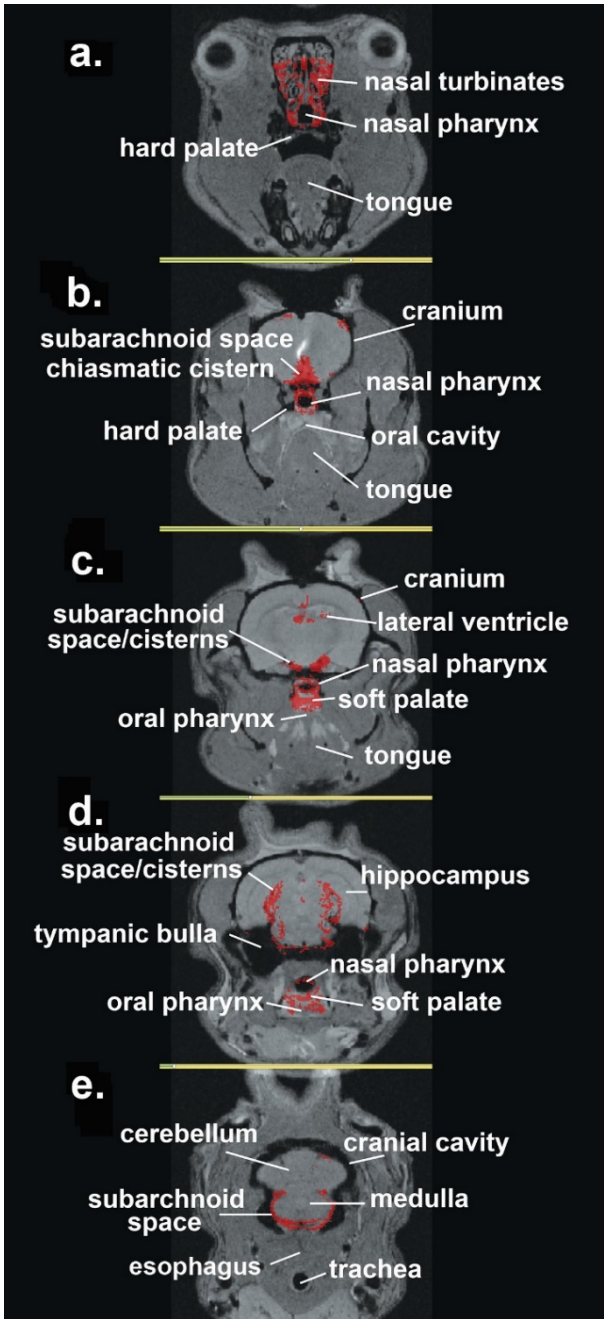

Figure 3. Fluorescent images of the lumen of the upper esophagus

Shown in the upper panel (a.) are photomicrographs of the lining of the esophagus from ex-vivo tissue taken at different times following ICV infusion of Qdots. Each time point displays two images from different areas of the esophagus. The 15 min sample was collected from a female rat infused with 10 µl of Qdots, while 30 and 35 min are from females infused with 20 µl of Qdots. The 40 min data were collected from a male infused with 10 µl of Qdots. The lower left panel (b.) shows photomicrographs of esophagus from a male rat infused with 10 µl of 0.9% NaCl (saline) taken with Zeiss LSM 880 confocal microscope held at the same fluorescent threshold as the other images. The lower right panel (c.) shows the presence of Qdots in the esophagus of a male rat following 1µl injections of Qdots into each nostril. White arrows point to the putative linear threads and strands of Qdot accumulating in mucus. Scale bar = 50 µm.

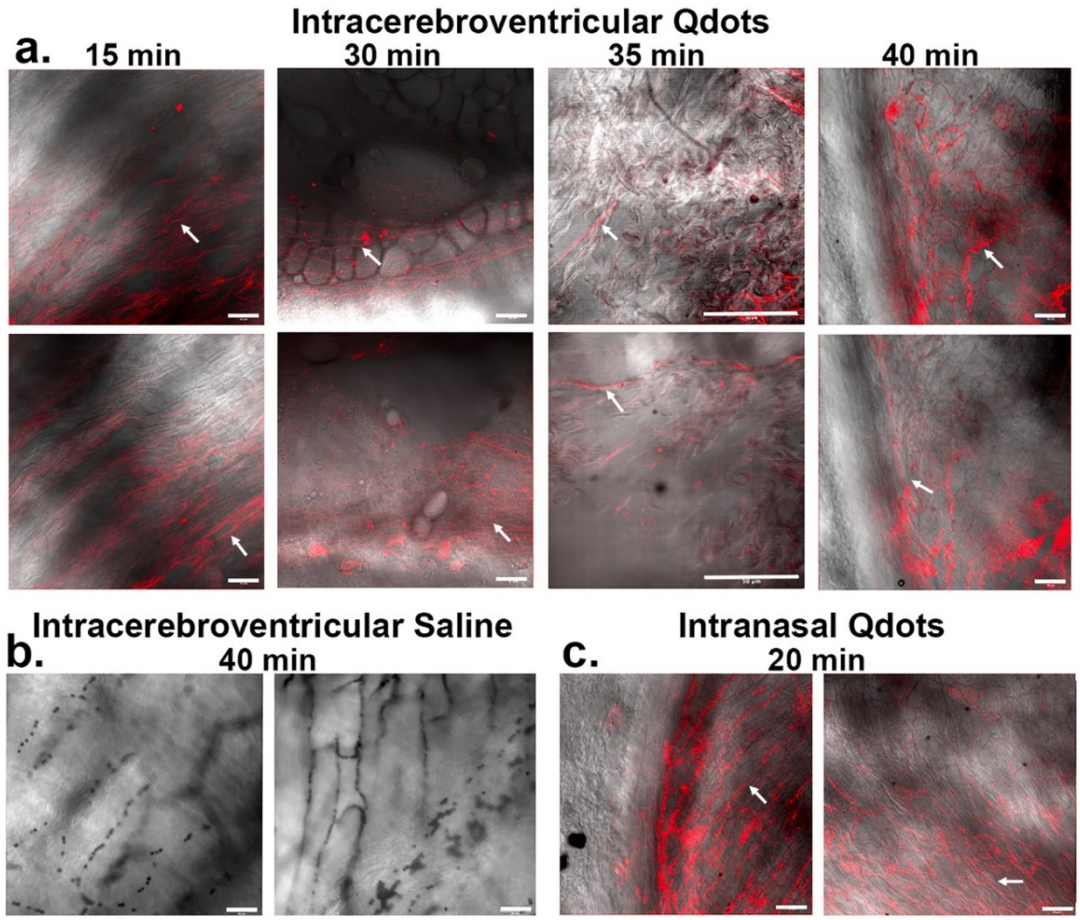

METHODS

Animals: Subjects were all adult Sprague Dawley rats (n = 13), approximately 100 days of age and purchased from Charles River Laboratories (Wilmington, MA, USA). Animals were housed in Plexiglas cages and maintained in ambient temperature (22–24°C) on a 12:12 light-dark cycle (lights on at 07:00 a.m.). Food and water were provided ad libitum. All methods and procedures described were approved by the Northeastern University Institutional Animal Care and Use Committee (IACUC). The Northeastern facility is AAALAC accredited with OLAW Assurance and is registered with the USDA. All housing, care, and use followed the Guide for the Care and Use of Laboratory Animals (8th Addition) and the Animal Welfare Act. The protocols used in this study adhere to the ARRIVE guidelines for reporting in vivo experiments in animal research (41)

Acclimation for Awake Imaging. All studies were done in awake rats to avoid the confound of anesthesia that impairs perivascular clearance (39). Rats underwent five days of consecutive acclimation. Rats were lightly anesthetized with isoflurane and placed into a copy of the restraining system used during awake imaging. When fully conscious, the animals were placed into a dark mock scanner tube with a sound recording of a standard MRI pulse sequence playing in the background. This acclimation procedure has been shown to significantly reduce plasma CORT, respiration, heart rate, and motor movements when compared with the first day of acclimation. The reduction in autonomic and somatic response measures of arousal and stress improves the signal resolution and MR image quality (42).

Surgical Procedure: Just prior to imaging, rats were anesthetized with 2 to 3% isoflurane and received an SC injection of the analgesic Metacam (meloxicam,5 mg/mL solution) at a dose of 1 mg/kg. The scalp was incised, and a burr hole was made in the skull for implantation of sterile PE10 tubing (Braintree Scientific) aimed at the right lateral cerebroventricle using the stereotaxic coordinates 1.0 mm posterior to the bregma, 2.0 mm lateral to the midline, and 4.0 mm in depth from dura. The tubing, ca 60 cm in length and prefilled with ferumoxytol (Feraheme^{TM} , 731-kD) contrast agent, was fixed in place with cyanoacrylic cement and

connected to a 0.3-mL syringe needle filled with the contrast agent that could be positioned just outside the bore of the magnet to give 10 µl of ferumoxytol (6 µg/µl Fe). This injection method has been used in previous studies to deliver drugs directly to the brain during awake imaging (43, 44). The surgery on rats maintained on the reversed light–dark cycle was performed under red-light illumination.

Imaging Acquisition: Rats were imaged within the first 4 h of the onset of the light–dark cycle. MRI was performed on a Bruker BioSpec 7-T/20-cm USR MRI spectrometer controlled by ParaVision 6.0 software. Radio frequency signals were sent and received with a custom quadrature volume coil built into the animal restrainer (Ekam Imaging Boston MA). Immediately after surgery, rats were quickly placed into the head coil and restraining system, a procedure that takes less than a minute (https://www.youtube.com/watch?v=JQX1wgOV3K4). The design of the restraining system includes a padded head support obviating the need for ear bars helping to reduce animal discomfort while minimizing motion artifact. Scans in both axial and sagittal views were collected before and after contrast agent administration. Quantitative-ultra-short-time-to-echo contrast enhanced (QUTE-CE) magnetic resonance imaging (MRI) technology was used to acquire data on CSF clearance in six subjects. A radial 3D UTE sequence implementation with acquisition parameters of TE/TR/FA =10 µs/4 ms/15°, BW=200 kHz, 3×3×3 cm^3 FOV, 180×180×180 matrix size, and 101,381 radial projections, were taken to produce 167 μm^3 isotropic resolution images, with a total scan time of 6 minutes and 45 seconds per image. A total volume of 10 µl of contrast agent was injected into the lateral ventricle at a rate of 1.6 µl/min using a syringe pump. This rate of injection is reported to keep intracranial pressure within a normal range (45).

Contrast-to-noise-ratio (CNR) maps as defined by signal-to-noise-ratio (SNR) post-contrast subtracted by SNR pre-contrast were co-registered to normalized space and generated with MATLAB as demonstrated in **Fig 1**. A region-of-interest within the field-of-view in air outside the head was used to obtain the standard deviation of the noise in calculating SNR. All other segmentations were rendered in 3D-Slicer. One subject underwent an additional 10 scans post-mortem, having died at the end of the imaging session while still in the scanner. These data were utilized to produce a high-resolution 3D segmentation irrespective to blood flow contributions and motion artifact.

Supplementary Data Fig 1S

See legend for Fig 1

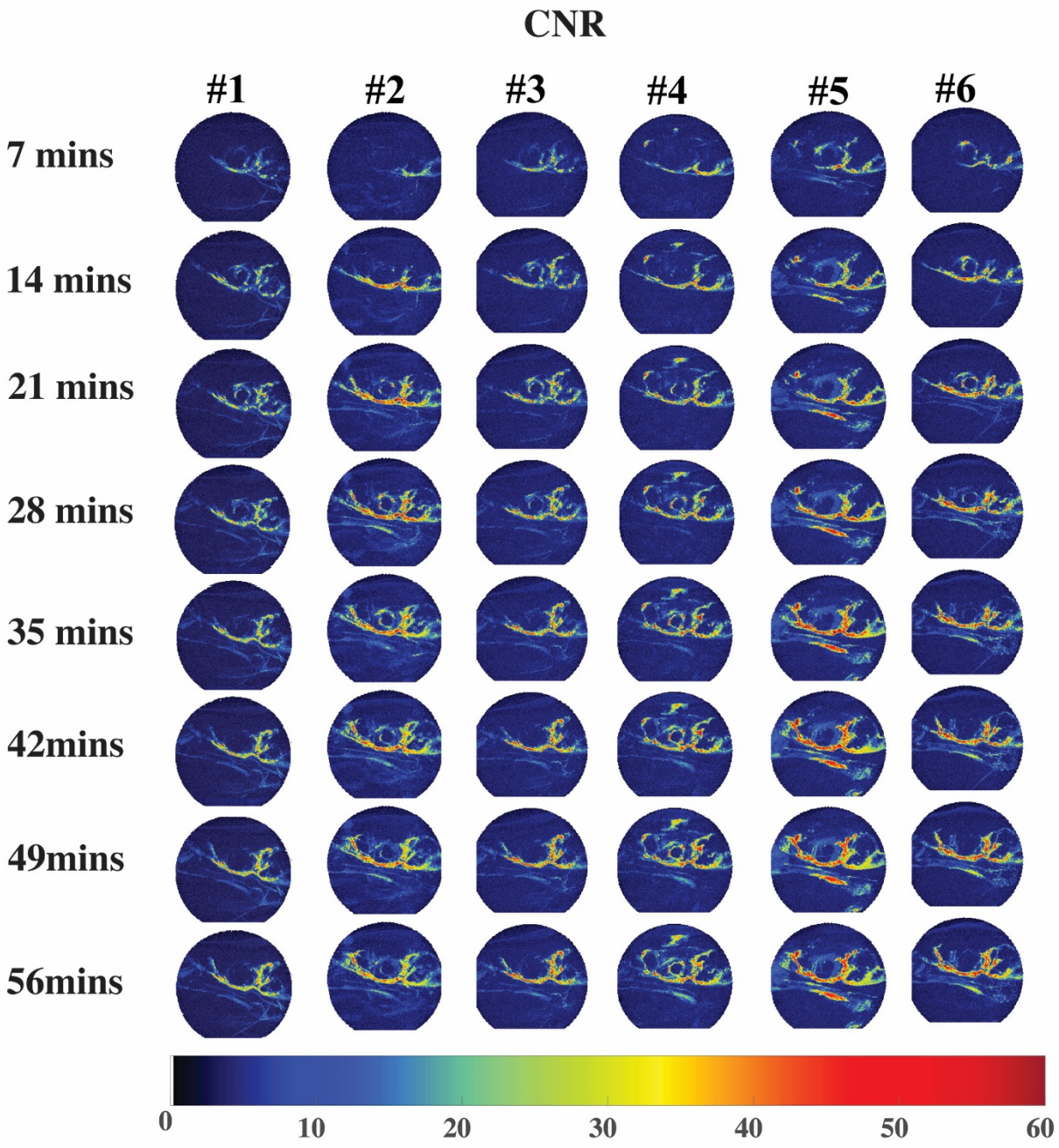

Supplementary Data Fig S2

See legend for Fig 2.

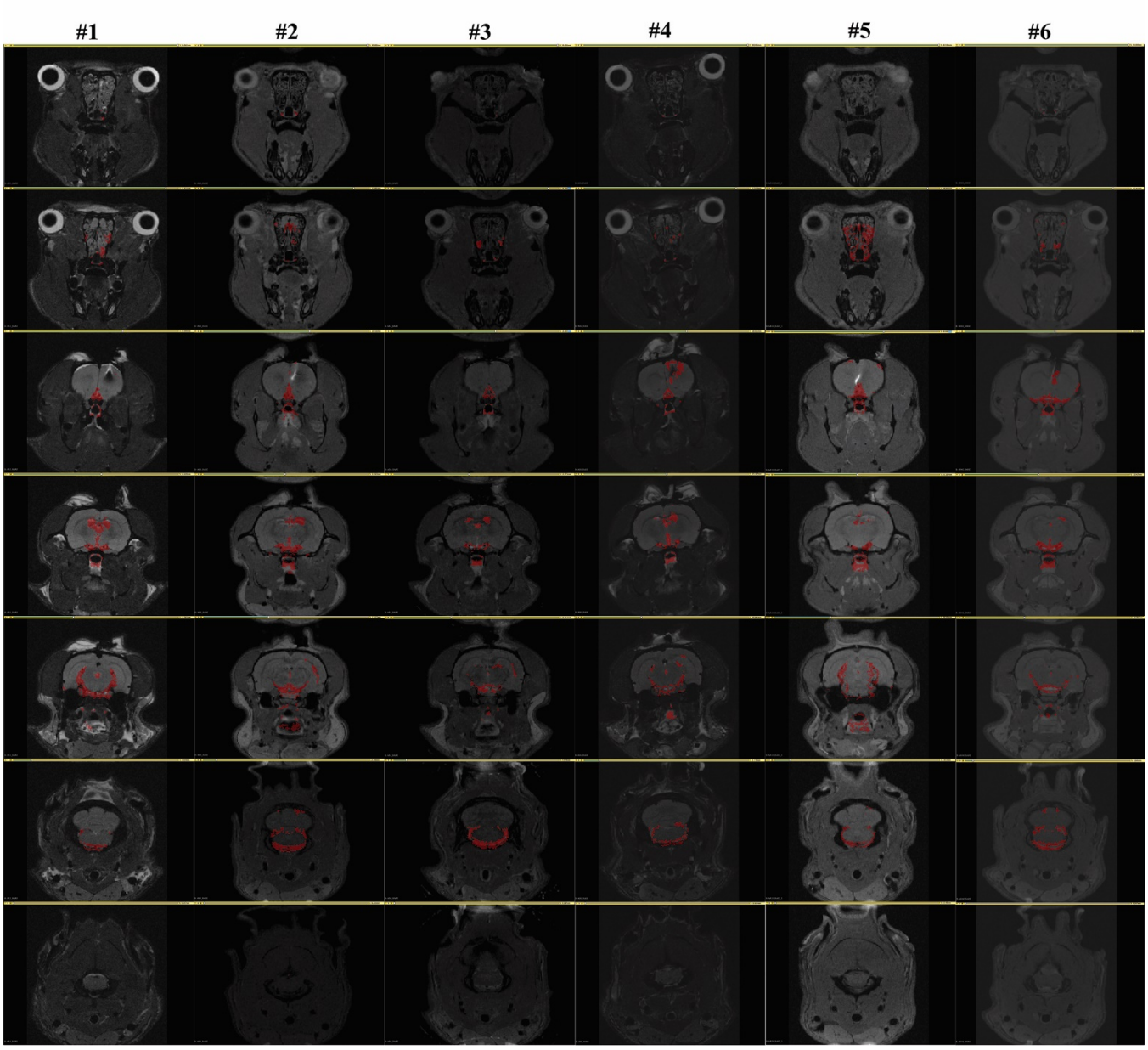

Supplementary Data Fig S3

Shown are photomicrographs of SPION contrast in the brain (NB), soft palate (SP), and oral pharynx (OP) following injections into the parenchyma (a.) or cerebroventricle (b.) T – trachea. Imaged modified from Muldoon et al 2004 (46).